ELSEVIER

Contents lists available at ScienceDirect

Biosensors and Bioelectronics

journal homepage: www.elsevier.com/locate/bios





A BTK-activatable targeted covalent NIR fluorescent probe for kinase monitoring and B-cell lymphoma imaging

Xinyue Zhao ^a, Yuxin Gu ^a, Yingyan Xie ^a, Naijie Wei ^a, Ziyang Fang ^a, Xiaowen Yan ^{a,b,*}, Qiuquan Wang ^a

- ^a Department of Chemistry and the MOE Key Laboratory of Spectrochemical Analysis & Instrumentation, College of Chemistry and Chemical Engineering, Xiamen University, Xiamen, 361005, China
- ^b Innovation Laboratory for Sciences and Technologies of Energy Materials of Fujian Province (IKKEM), Xiamen, 361005, China

ARTICLE INFO

Keywords: Fluorescence probe Targeted covalent inhibitor Bruton's tyrosine kinase Cancer imaging B-Cell lymphoma

ABSTRACT

B-cell lymphoma is one of the most aggressive malignancies worldwide. Bruton's tyrosine kinase (BTK), a crucial mediator of B-cell receptor (BCR) signaling pathway, has emerged as a pivotal therapeutic target for B-cell lymphoma, so developing a molecular probe capable of quantitatively monitoring BTK expression and activity in live cells would be highly desirable for the early diagnosis and therapy of B-cell lymphoma. Here, we have constructed a BTK-activatable NIR fluorescent (NIRF) probe (Ibt-CyOH), which features a targeting ligand of ibrutinib as a recognition unit, a NIRF reporter, and an α -methylated acrylamide as a cleavable linker, triggered by nucleophilic addition–elimination reactions. Ibt-CyOH demonstrates high selectivity and inhibitory potency against BTK. A significant "turn-on" NIR fluorescence is generated upon the covalent binding of Ibt-CyOH to BTK, enabling real-time imaging of B-cell lymphoma cells as well as BTK inhibition in living mice. Our work establishes a promising targeted covalent activation strategy and provides a novel targeted covalent NIR probe for imaging of BTK in vivo, which will be beneficial to the diagnosis and treatment of B cell malignancies and will inspire the development of new NIRF probe in the future by redesigning the numerous targeted covalent drugs approved by FDA.

1. Introduction

Bruton's tyrosine kinase (BTK), a crucial member of the Tec family non-receptor tyrosine kinases, acts as a central mediator in the B-cell receptor (BCR) signaling pathway (Aoki et al., 1994; Khan, 2001). The BCR pathway coordinates essential cellular functions including proliferation, differentiation, apoptotic regulation, and chemotactic responses, while serving as a critical regulator in the pathogenesis of various B-cell malignancies (Satterthwaite et al., 1997). Consequently, BTK is essential for sustaining cellular survival and promoting proliferation in multiple B-cell malignancies and autoimmune disorders, including diffuse large B-cell lymphoma (DLBCL), B-cell chronic lymphocytic leukemia (CLL), follicular lymphoma (FL) and mantle-cell lymphoma (MCL). Therefore, it is critical to develop novel approaches that enable precise, real-time detection of both BTK expression and its activity in living cells, which holds significant implications for the diagnosis and treatment of B-cell malignancies (Buggy and Elias, 2012).

Fluorescent prodrugs have recently gained significant attention in

cancer management owing to its ability to provide non-invasive diagnostic information while simultaneously offering therapeutic potential (Li et al., 2019; Sharma et al., 2024; Wang et al., 2018). Near-infrared fluorescent (NIRF) probes are advanced chemical tools for live cell imaging and disease diagnosis, thanks to their ability to image deep tissues non-invasively with excellent sensitivity and minimal autofluorescence interference (Ceballos-Ávila et al., 2024; Chen et al., 2022; Hong et al., 2017; Owens et al., 2016). Consequently, fluorescent prodrugs equipped with NIRF probes as optical reporters have gained interest for cancer fluorescence diagnosis and for real-time monitoring of prodrug activation in vivo (Kumar et al., 2015; Li et al., 2022; Yin et al., 2021). Previously reported fluorescent prodrugs generally consist of an NIR fluorophore linked to a masked chemotherapy drug (Han et al., 2023; Zhang et al., 2020) (e.g., doxorubicin (Christidi and Brunham, 2021; Li et al., 2023), camptothecin (Kamle et al., 2024), and paclitaxel (Zhu and Chen, 2019)), with both the drug and fluorophore being released within the tumor microenvironment, triggered by factors such as reactive oxygen species (Deng et al., 2025; Liu et al., 2017; Xue et al., 2025),

^{*} Corresponding author. Innovation Laboratory for Sciences and Technologies of Energy Materials of Fujian Province (IKKEM), Xiamen, 361005, China. *E-mail address:* xwyan@xmu.edu.cn (X. Yan).

hypoxia (Song et al., 2024; Zhao et al., 2021), GSH (Cao et al., 2025; Wu et al., 2014; Ye et al., 2016), acidic pH (Liu et al., 2023) and enzyme (Cao et al., 2024; Chen et al., 2023; Wang et al., 2024; Wei et al., 2024) (Scheme 1a).

Herein, we propose a novel strategy for activating NIRF probe via a targeted covalent binding-induced nucleophilic addition-elimination reaction. The designed NIRF probe consists of a targeting ligand, an electrophilic warhead (EW), and an NIR fluorophore (Scheme 1b). Upon encountering the target protein, the targeting ligand interacts specifically with the protein, bringing the EW into close proximity to the nucleophilic group (Nu) of the amino acid residue near the ligandbinding site. The nucleophilic addition-elimination reaction then occurs between the EW and Nu, forming a covalent bond between the EW and the kinase, followed by the release of a fluorophore. Ultimately, this strategy enables targeted covalent inhibition of the protein target and simultaneous "turn-on" fluorescence imaging of the tumor (Scheme 1b). An ideal targeted covalent activatable theranostic fluorescent probe should meet the following criteria: (1) high specificity for recognizing target proteins (single-source activation); (2) high inhibitory potency due to covalent inhibition; (3) rapid release of the fluorophore with high efficiency; and (4) turn-on NIRF for non-invasiveness in vivo tumor imaging.

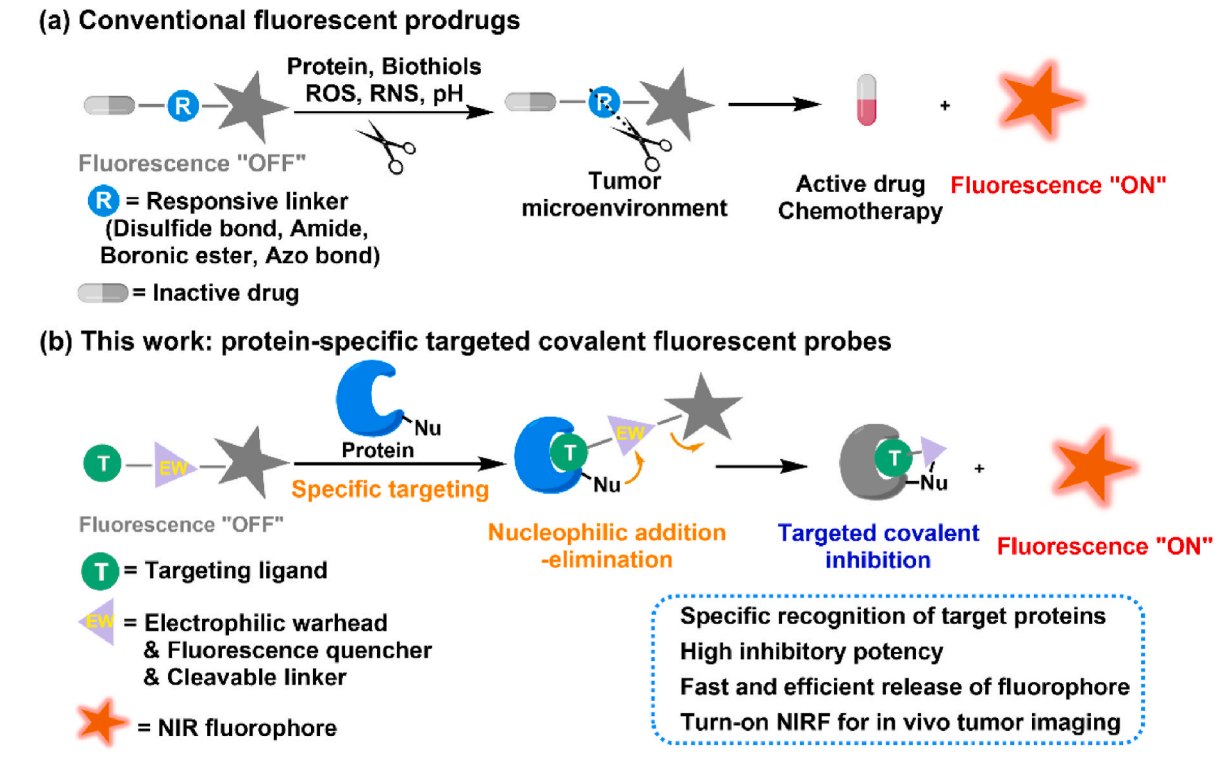
In this study, we selected ibrutinib, a targeted covalent inhibitor (TCI) (Lonsdale and Ward, 2018) of BTK, has been approved by the US Food and Drug Administration (FDA) as a breakthrough therapeutic for B-cell malignancies. Ibrutinib consists of a specific targeting ligand and an acrylamide EW that covalently reacts with Cys481 near the ATP-binding pocket of BTK, thereby inhibiting its activity and biological functions (Pan et al., 2007; Wang Michael et al., 2023). Several fluorescence probes based on ibrutinib have been reported for BTK imaging in live cells (Kim et al., 2015; Liu et al., 2015; Zhang et al., 2014). However, studies on "off-on" NIRF probe for in vivo BTK imaging and targeted killing of B-cell malignancies cells are still lacking.

We designed a BTK-targeting and activatable NIRF probe (Ibt-CyOH) $\,$

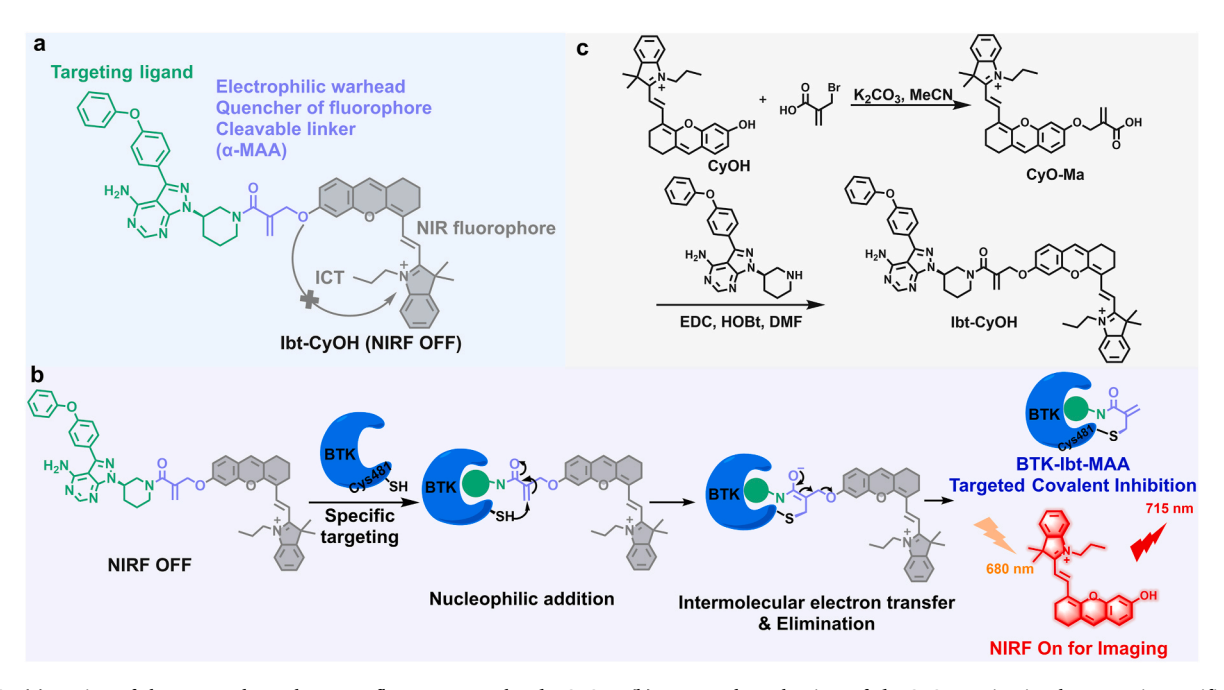
(Scheme 2a), which includes a targeting ligand of ibrutinib as the recognition unit for BTK, a NIR fluorophore (hemicyanine, CyOH (Wu et al., 2016)) as the NIRF reporter, and an α -methylated acrylamide (α-MAA) group (Reddi et al., 2021; Zhuang et al., 2020) as the linker. The α-MAA serves "four-in-one" functions: 1) an EW, 2) a bridge connecting the targeting ligand and fluorophore, 3) a quencher of the NIR fluorophore by suppressing the intramolecular charge transfer (ICT) effect (Tseng et al., 2021; Zhou et al., 2024) of CvOH, and 4) a cleavable linker induced by the nucleophilic addition-elimination reaction. Although Reddi and coworkers developed a fluorescence probe (3k) of BTK based on the substituted methacrylamide, probe 3k was confined to validate the proposed mechanism of covalent ligand directed release. Herein, we developed the BTK-targeting and activatable NIRF probe (**Ibt-CyOH**) to expand the applications of α-methylated acrylamide for selective detection of BTK in live cells and in vivo imaging of B-cell lymphoma.

As shown in Scheme 2b, upon encountering BTK, the targeting ligand of Ibt-CyOH interacts specifically with BTK, bringing the α -

MAA near Cys481 close to the ligand binding site, resulting in a high local concentration. The sulfhydryl group of Cys481 then nucleophilically attacks the C=C bond of α -MAA, generating 1,4-addition enol intermediates, in which the elimination reaction occurs owing to intramolecular electron transfer. Generally, the nucleophilic addition-elimination reaction leads to the formation of a covalent bond between α -MAA and BTK (BTK-Ibt-MAA), followed by the release of CyOH, concomitant with the "turn-on" NIRF due to the recovery of the ICT effect. In this manner, targeted covalent inhibition and "turn-on" fluorescence BTK imaging are realized simultaneously. Scheme 2c presents the synthesis route of Ibt-CyOH, CyOH, obtained according to previous literature (Wu et al., 2016), was reacted with 2-(bromomethyl) acrylic acid in the presence of K₂CO₃ to afford CyO-Ma (Scheme S1). Ibt-CyOH was then prepared via an amide condensation reaction between CyO-Ma and the targeting ligand of ibrutinib (Scheme S2). Detailed synthetic steps and characterization of the above compounds



Scheme 1. (a) Previously reported activatable fluorescent prodrugs consisting of an NIR fluorophore linked to a masked chemotherapy drug, released within the tumor microenvironment. (b) Schematic illustrating the activation process of a targeted covalent fluorescent probe through specific protein-binding-triggered nucleophilic addition–elimination reaction, resulting in targeted covalent inhibition and simultaneous "turn-on" fluorescence imaging of the protein target.



Scheme 2. (a) Design of the targeted covalent NIR fluorescent probe Ibt-CyOH. (b) Proposed mechanism of Ibt-CyOH activation by BTK via specific binding-triggered nucleophilic addition—elimination reaction for targeted covalent inhibition and "Off—On" NIRF imaging. (c) Synthetic route of Ibt-CyOH.

are provided in Figs. S1-9.

2. Experimental section

Experimental section including reagents, experimental equipment, experimental details, characterization and detection were presented in Supporting Information.

3. Results and discussion

3.1. Optical response of Ibt-CyOH towards recombinant BTK

We first investigated the optical response of Ibt-CyOH to recombinant BTK. As shown in Fig. 1a and S12a, Ibt-CyOH displayed absorption peak at 592 nm and its fluorescence intensity is weak. Upon adding recombinant BTK (2 µM), a red shift to 681 nm was observed, accompanied with a color change of the solution from blue-violet to cyan (Fig. 1a). Meanwhile, NIRF intensity at 715 nm significantly increased with a 42-fold fluorescence intensity enhancement within 2 min, indicating a high and rapid signal response of Ibt-CyOH to BTK (Fig. 1a, b, c). Due to experimental procedures such as analytes addition and thorough mixing, the time interval for the kinetic study was set as 2 min. Additionally, a strong linear relationship was observed between fluorescence intensity and the concentration of recombinant BTK from 0.2 to 2 μ M, with a limit of detection (LOD) of 27 nM (LOD = $3\sigma/k$, S/N = 3), demonstrating the high sensitivity of Ibt-CyOH to recombinant BTK (Fig. 1d). In contrast, the fluorescence response to 10 mM GSH was very slow, suggesting low reactivity of Ibt-CyOH with GSH, which lacks a targeting group. After adding the BTK solution pre-treated with ibrutinib to Ibt-CyOH solution, there was also no obvious change in the fluorescence intensity at 715 nm (Fig. 1e). Upon adding recombinant BTK and GSH, notable fluorescence intensity change was observed as shown in Fig. 1e. The fluorescence changes in Ibt-CyOH towards various biologically relevant species, such as BSA, HSA, GSH, amino acids (Cys, Hcy, Ser, Tyr, Glu, His, Met, Thr, Arg, Lys), metal ions (K⁺, Na⁺, Ca²⁺, Cu²⁺, Fe^{3+}), SO_3^{2-} , H_2O_2 , HCIO, H_2S , DTT was shown in Fig. 1f. The relevant species cannot induce significant fluorescence changes, indicating the high selectivity of Ibt-CyOH toward BTK. These results suggest that our probe can be sensitively and specifically activated by BTK, even in the

presence of a high concentration of GSH, making it favorable for living cell imaging.

3.2. Recognition mechanism of Ibt-CyOH towards BTK

To study the reaction mechanism between Ibt-CyOH and sulfhydryl, HPLC-MS was used to analyze the reaction products of Ibt-CyOH and GSH in potassium phosphate buffer (100 mM, pH 8.0, 37 °C) for a long reaction time (24h) (Fig. S10). We speculated that GSH first nucleophilically attacks **Ibt-CyOH**, resulting in the formation of 1,4-addition intermediates, which could then undergo Path A (nucleophilic addition-elimination reaction) to generate substitution products, along with the release of CyOH, or Path B (nucleophilic addition without elimination) to generate the undesired addition products. As shown in Fig. S11, the expected substitution products (Ibt-MAA-GSH, $[M+H]^+$, m/z, 760; and [M-H], m/z, 758) and the NIR fluorophore CyOH (M⁺, m/z, 412) were detected with high intensity, while the undesired addition product $(M^+, m/z, 1171.5)$ was not observed. These results demonstrate that **Ibt**-CyOH undergoes the expected nucleophilic addition-elimination reaction pathway toward sulfhydryl (Fig. S10). Therefore, the NIR CyOH was generated efficiently, consistent with the observed high fluorescence response of Ibt-CvOH toward BTK.

To further explore the reaction mechanism and the covalent binding site of **Ibt-CyOH** with BTK (Scheme 2b), we performed HPLC-ESIMS-based peptide mapping to identify stable adduct formation between the **Ibt-CyOH** and tryptic peptide. The **Ibt-CyOH**-labeled BTK was subjected to following trypsin digestion procedures including protein reduction with DTT, iodoacetamide (IAA) alkylation, and trypsin digestion, followed by HPLC-ESIMS-based peptide mapping. Consistent with our expectations, MS/MS fragmentation of Ibt-MAA-labeled peptide fragment 467–487 (QRPIFIITEYMANGC(Ibt-MAA)LLNYLR) was determined in Fig. S12a. Ibt-MAA-labeled peptide 467–487 (QRPIFIITEYMANGC(Ibt-MAA)LLNYLR, [M+3H] $^{3+}$, m/z, 994.2094; [M+4H] $^{4+}$, m/z, 745.9110; calculated [M+3H] $^{3+}$, m/z, 994.1680; [M+4H] $^{4+}$ m/z, 745.8760) was detected (Fig. S12c and d), indicating that Cys481 is the specific covalent binding site of **Ibt-CyOH** on BTK.

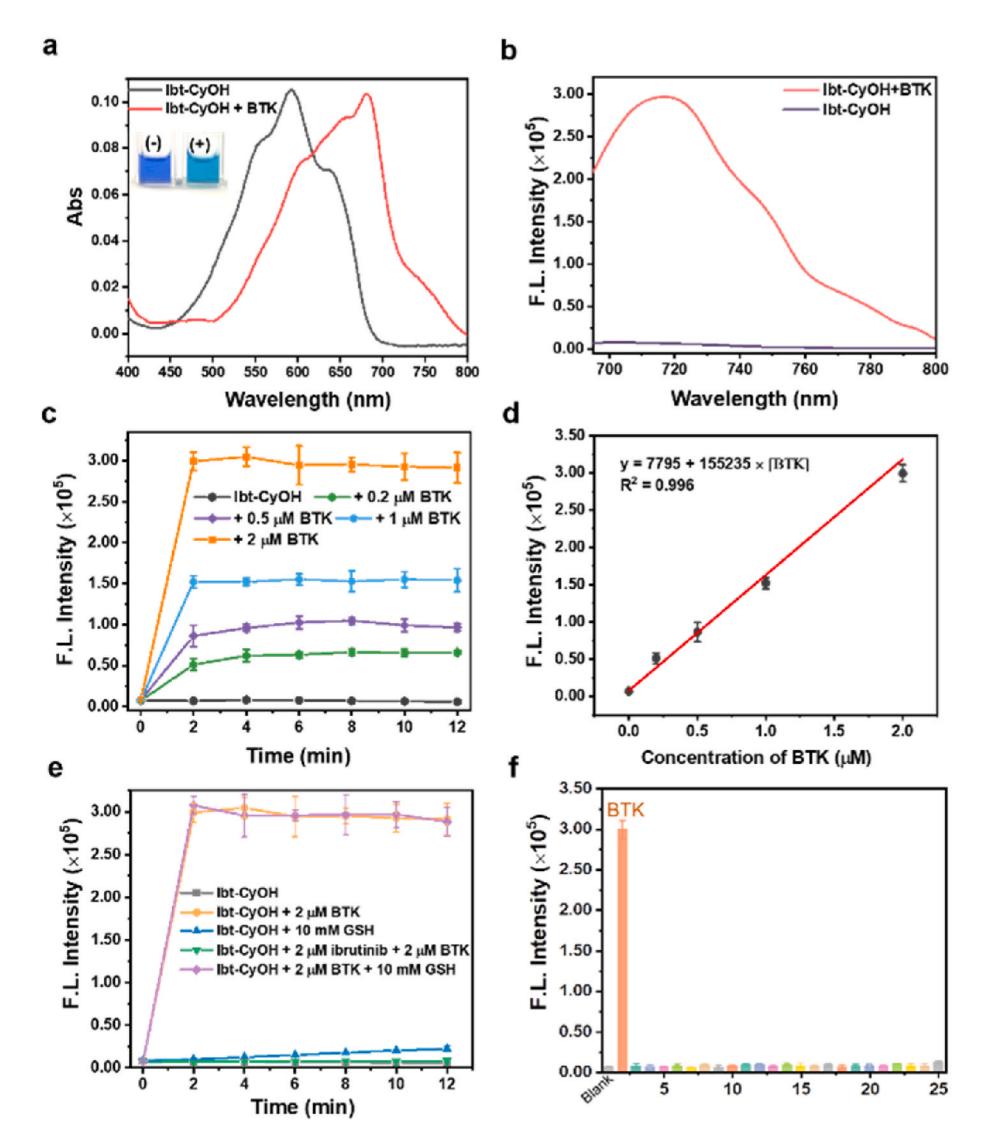


Fig. 1. (a) Absorption and (b) Fluorescence spectra of Ibt-CyOH (2 μ M) in the presence of recombinant BTK (2 μ M). (c) Time-dependent fluorescence response of Ibt-CyOH (2 μ M) to different concentrations of recombinant BTK (0.2, 0.5, 1, 2 μ M) at 715 nm. (d) Linear fitting curve of fluorescence intensity response of Ibt-CyOH (2 μ M) with or without analytes (BTK, GSH, ibrutinib). (e) Time-dependent fluorescence response of Ibt-CyOH (2 μ M) with or without analytes (BTK, GSH, ibrutinib). (f) Fluorescence intensity of Ibt-CyOH (2 μ M) toward various analytes (100 μ M) including BTK, BSA, HSA, GSH, Cys, Hcy, Ser, Tyr, Glu, His, Met, Thr, Arg, Lys, K⁺, Na⁺, Ca²⁺, Cu²⁺, Fe³⁺, SO₃²⁻, H₂O₂, HCIO, H₂S, DTT. Data are shown as mean \pm SD (n = 3).

3.3. In situ reactivity and selectivity of Ibt-CyOH towards BTK

We further applied a competitive binding assay to evaluate the reactivity of Ibt-CvOH toward recombinant and cellular BTK in OCI-LY10 cells (Degorce et al., 2018), a human cell line derived from activated B-cell-like diffuse large B-cell lymphoma. PCI-33380 (Bodipy-modified ibrutinib derivative) (Honigberg et al., 2010), an irreversible fluorescence probe of BTK (Fig. 2a), was used. PCI-33380 formed stable adducts with both recombinant and cellular BTK after 1 h of incubation (DMSO lane, Fig. 2b). A concentration-dependent competitive binding of Ibt-CyOH to recombinant BTK was observed, with 150 nM Ibt-CyOH effectively occupying recombinant BTK (150 nM). Meanwhile, pretreatment of OCI-LY10 cells with Ibt-CyOH (100 nM) completely eliminated the PCI-33380-labeled BTK band, while 50 nM ibrutinib completely occupied intracellular BTK (Fig. 2b). The above experiments indicated that Ibt-CyOH has good in situ reactivity toward BTK; however, its efficacy is lower than that of ibrutinib. We speculated that the methylation at the α site of acrylamide increases the electron cloud density of α , β -unsaturated ketone, weakening its electrophilic reactivity to BTK. Therefore, the addition reaction is less likely to occur, which

may explain why ${\bf Ibt\text{-}CyOH}$ shows weaker inhibitory activity compared with ibrutinib.

To further demonstrate the in situ selectivity and activity of Ibt-CVOH toward BTK, we evaluated its inhibitory effect on the BTKmediated BCR signaling pathway in OCI-LY10 cells through SDS-PAGE immunoblotting. BTK is a key regulator of the BCR signaling pathway, affecting the proliferation, survival, and other activities of B cells (Pal Singh et al., 2018) (Fig. 2c). We used anti-IgM (a mimic of BCR-antigen) to stimulate the phosphorylation of BTK and its upstream (Syk) and downstream kinases (PLC₇2, Erk1/2) along the BCR signaling pathway (Woyach et al., 2012) (Fig. 2c). As shown in Fig. 2d, Ibt-CyOH specifically inhibited the phosphorylation of BTK as well as its downstream kinases (PLCγ2, Erk1/2) in a concentration-dependent manner, and 200 nM Ibt-CyOH was found to completely inhibit the phosphorylation of these kinases. However, the phosphorylation of the upstream kinase Syk was not affected. These results indicated the high in situ selectivity and inhibiting activity of Ibt-CyOH toward the BTK-mediated BCR signaling pathway.

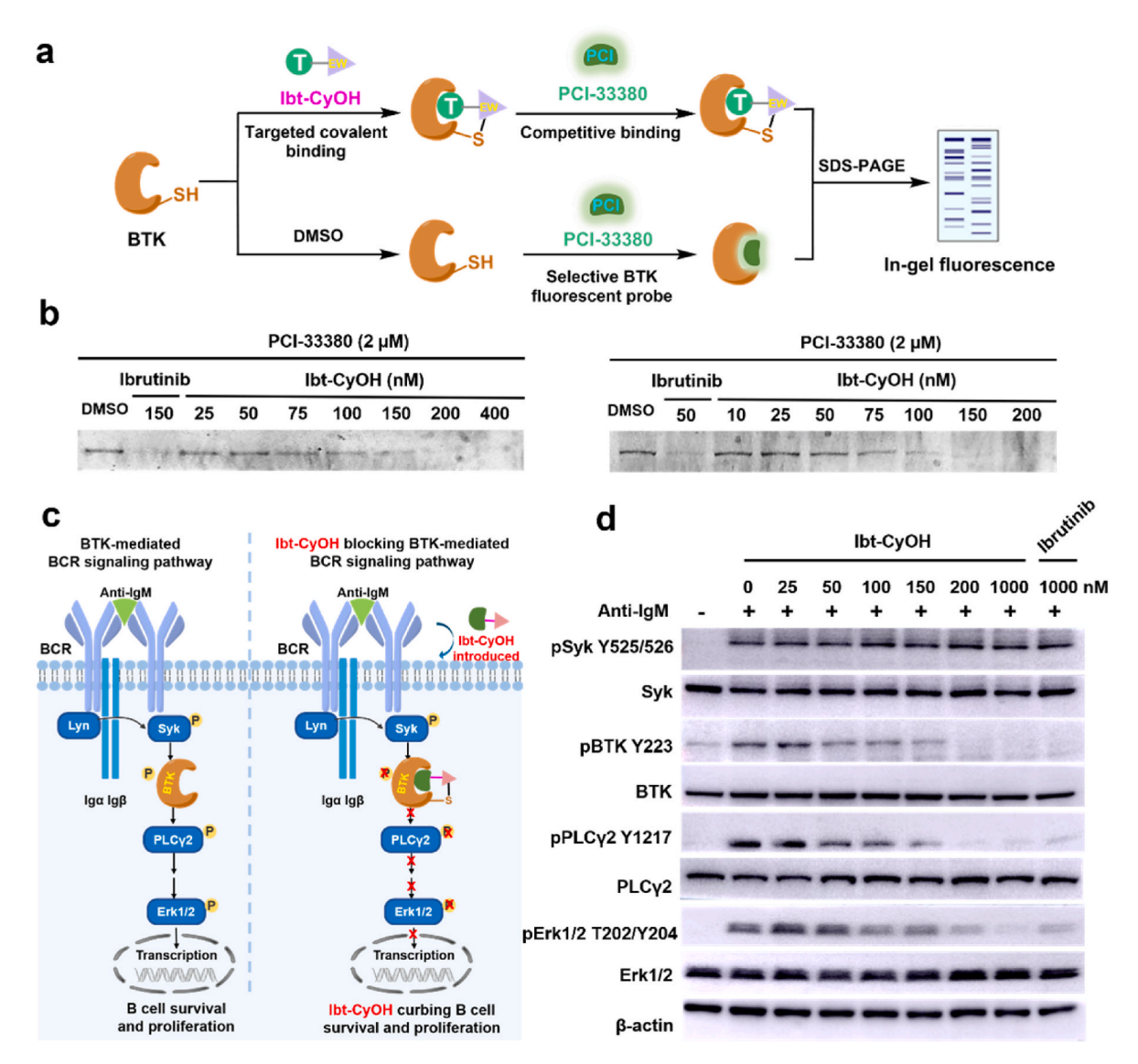


Fig. 2. (a) Schematic illustrating the principle of the competitive binding assay. (b) Concentration-dependent binding of **Ibt-CyOH** to (left) recombinant BTK (150 nM) and (right) BTK in OCI-LY10 cells through the competitive binding assay using PCI-33380. (c) Schematic illustrating the BTK-mediated BCR signaling pathway and its inhibition by **Ibt-CyOH**. (d) Concentration-dependent inhibition of BCR phosphorylation signaling in OCI-LY10 cells by **Ibt-CyOH**, as determined by SDS-PAGE immunoblotting. The corresponding uncropped images of gels and blots are shown in Figs. S13 and 14.

3.4. Ibt-CyOH for NIRF imaging of BTK in living cells

Having proven the optical response, as well as in situ selectivity and activity of Ibt-CyOH, we further explored its ability for BTK imaging in OCI-LY10 cells (BTK+). Jurkat cells (a human T lymphocyte cell line) that do not express BTK were chosen as a negative control (Kraft et al., 2021). As shown in Fig. 3a, after incubation with Ibt-CyOH (2 μ M) for 30 min, evident red fluorescence signals were observed in OCI-LY10 cells. In contrast, negligible red fluorescence signals were observed after incubation with Ibt-CyOH (2 μ M) in Jurkat cells (BTK-) for 90 min (Fig. 3b). To ensure that the observed red fluorescence specifically originated from endogenous BTK, we used ibrutinib and PCI-33380 in a competitive binding experiment. We found that ibrutinib-pretreated OCI-LY10 cells, when subsequently incubated with Ibt-CyOH (2 µM), did not exhibit fluorescence in the red channel (Fig. 3a-c). In contrast, cells pretreated with PCI-33380 exhibited evident green fluorescence, while weak red fluorescence from Ibt-CyOH was observed. These data suggest that the turn-on NIRF response is specifically triggered by the endogenous BTK. To further explore the distribution of CyOH in OCI-LY10 cells activated by BTK, we conducted colocalization fluorescence imaging assays using MitoTracker green to stain mitochondria (Fig. 3d). The results indicated that the activated NIRF signals in OCI-LY10 cells (suspension cells) correlated well with MitoTracker green, with a high Pearson's correlation coefficient of 0.85, calculated using ImageJ software (Fig. 3d). This suggests that the released CyOH accumulated in the mitochondria. The above results show that BTK specifically and effectively activates Ibt-CyOH and that the released CyOH accumulates in the mitochondria, enabling real-time and in situ NIRF imaging of BTK in living B-cell malignancy cells.

3.5. Antiproliferative activity of Ibt-CyOH to B-cell malignancy cells

Having proven that **Ibt-CyOH** can covalently bind to BTK and inhibit the BTK-mediated BCR signaling pathway, the inhibitory potency of **Ibt-CyOH** against B-cell malignancy cells was evaluated using standard CCK-8 assays. We chose OCI-LY10 and Ramos cells (Burkitt's lymphoma cells, BTK+) as model cancer cells. As shown in Fig. 4a–c, the half-maximal inhibitory concentrations (IC $_{50}$, μ M) of **Ibt-CyOH** against OCI-LY10 and Ramos cells were determined to be 1.89 and 14.11 μ M, respectively. Similarly, the IC $_{50}$ of ibrutinib against OCI-LY10, Ramos

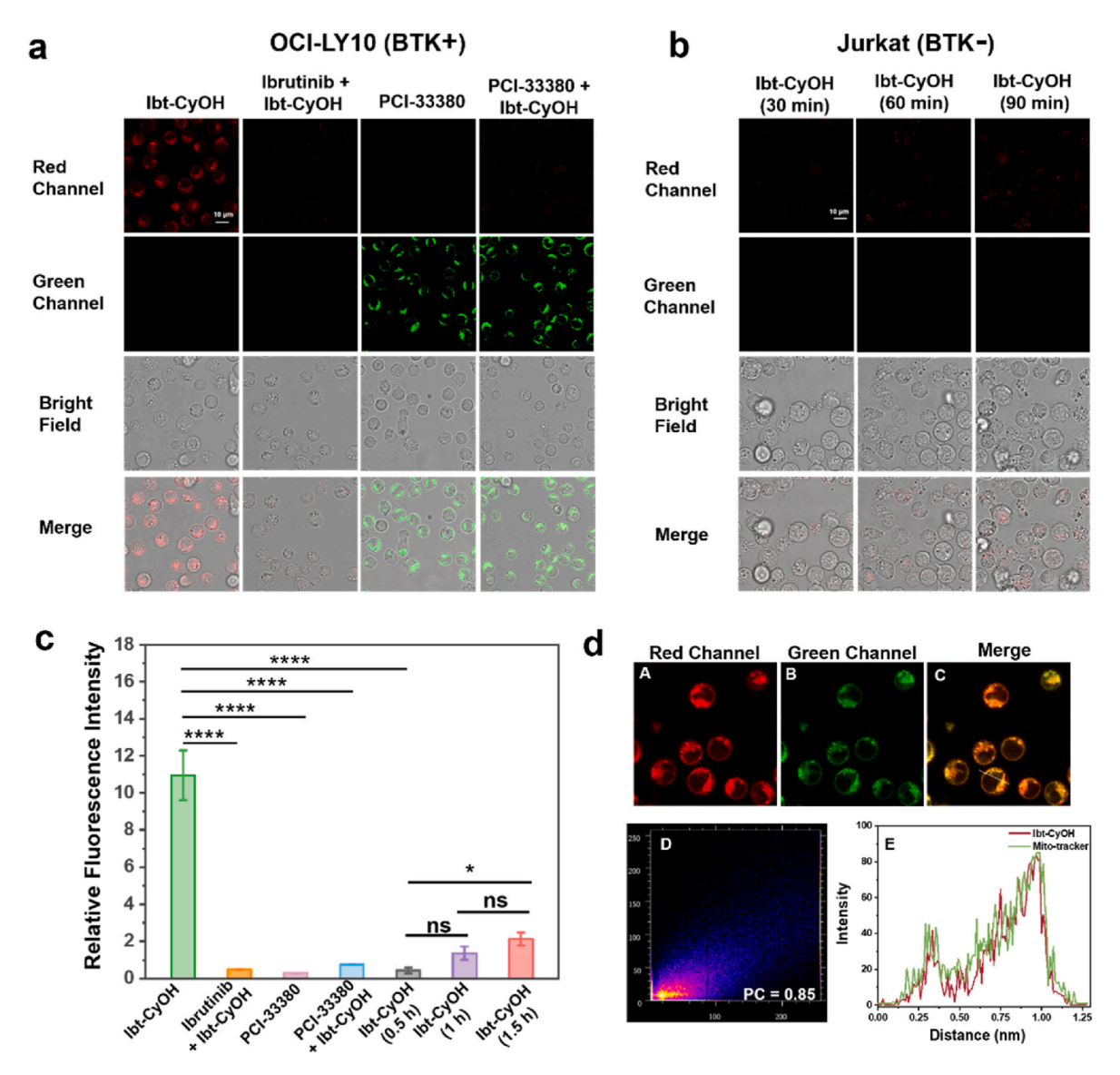


Fig. 3. Confocal fluorescence images in OCI-LY10 (a) and Jurkat (b) cells. (a) left to right: OCI-LY10 cells incubated with Ibt-CyOH (2 μM) for 0.5 h; Cells pretreated with ibrutinib (20 μM) for 1 h, followed by subsequent incubation with Ibt-CyOH (2 μM) for 0.5 h; Cells incubated with PCI-33380 (10 μM) for 1 h; Cells pretreated with PCI-33380 (10 μM) for 1 h and then treated with Ibt-CyOH (2 μM) for 0.5 h. (b) Jurkat cells treated with Ibt-CyOH (2 μM) for 0.5 h, 1 h, and 1.5 h. Green channel: $\lambda_{ex} = 488$ nm, $\lambda_{em} = 535 \pm 35$ nm; red channel: $\lambda_{ex} = 638$ nm, and $\lambda_{em} = 715 \pm 35$ nm. (c) Relative fluorescence intensity of the corresponding fluorescence images of the red channel in (a, b); results are expressed as mean \pm SD (n = 3), statistical significance is determined by ANOVA tests: *P < 0.05, ****P < 0.0001, ns, no statistically significant difference. (d) Confocal microscopic images of colcalized experiments in OCI-LY10 cells. Fluorescence images of OCI-LY10 cells with Ibt-CyOH (2 μM) for 1 h (panel A) and fluorescence images of OCI-LY10 cells treated with MitoTracker green (panel B). Panel C: the overlay of merged images of panels A and B. Panel D: the correlation between Ibt-CyOH and MitoTracker green. Panel E: fluorescence intensity profile of regions of interest (white line in panel C). Green channel: $\lambda_{ex} = 488$ nm, $\lambda_{em} = 516 \pm 15$ nm; red channel: $\lambda_{ex} = 638$ nm, $\lambda_{em} = 715 \pm 35$ nm. (For interpretation of the references to color in this figure legend, the reader is referred to the Web version of this article.)

cells were determined to be 1.40 and 10.62 μ M, suggesting that OCI-LY10 cells are more sensitive to both Ibt-CyOH and ibrutinib than Ramos cells. The effectiveness of Ibt-CyOH in OCI-LY10 cells was further evaluated through Live/Dead cell staining using a Calcein-AM/PI kit, as Calcein-AM can be hydrolyzed by esterases in living cells to generate the green, fluorescent Calcein, while PI stains the DNA double helix in dead cells, producing red fluorescence. As shown in Fig. 4d, when treated with PBS, OCI-LY10 cells remained alive and emitted green fluorescence from Calcein. In contrast, bright red and weak green fluorescence were observed in OCI-LY10 cells treated with Ibt-CyOH, further validating the inhibition effects. These experimental results indicate that Ibt-CyOH has high antiproliferative activity to B-cell malignancy cells.

3.6. Ibt-CyOH for NIRF imaging of BTK in vivo

We further focused on BTK imaging in living mice using **Ibt-CyOH**. MCID mice carrying OCI-LY10 cells xenograft tumors with an initial volume of approximately 100 mm³ were used for in vivo BTK imaging. As shown in Fig. 4e, the real-time fluorescence images showed that the NIRF signal in the tumor region gradually increased and reached a plateau at 1 h. Additionally, pre-treating the tumor with ibrutinib efficiently blocked the NIRF emission (Fig. 4f and g), indicating that **Ibt-CyOH** has the ability for specific and real-time imaging of B-cell malignancies in vivo.

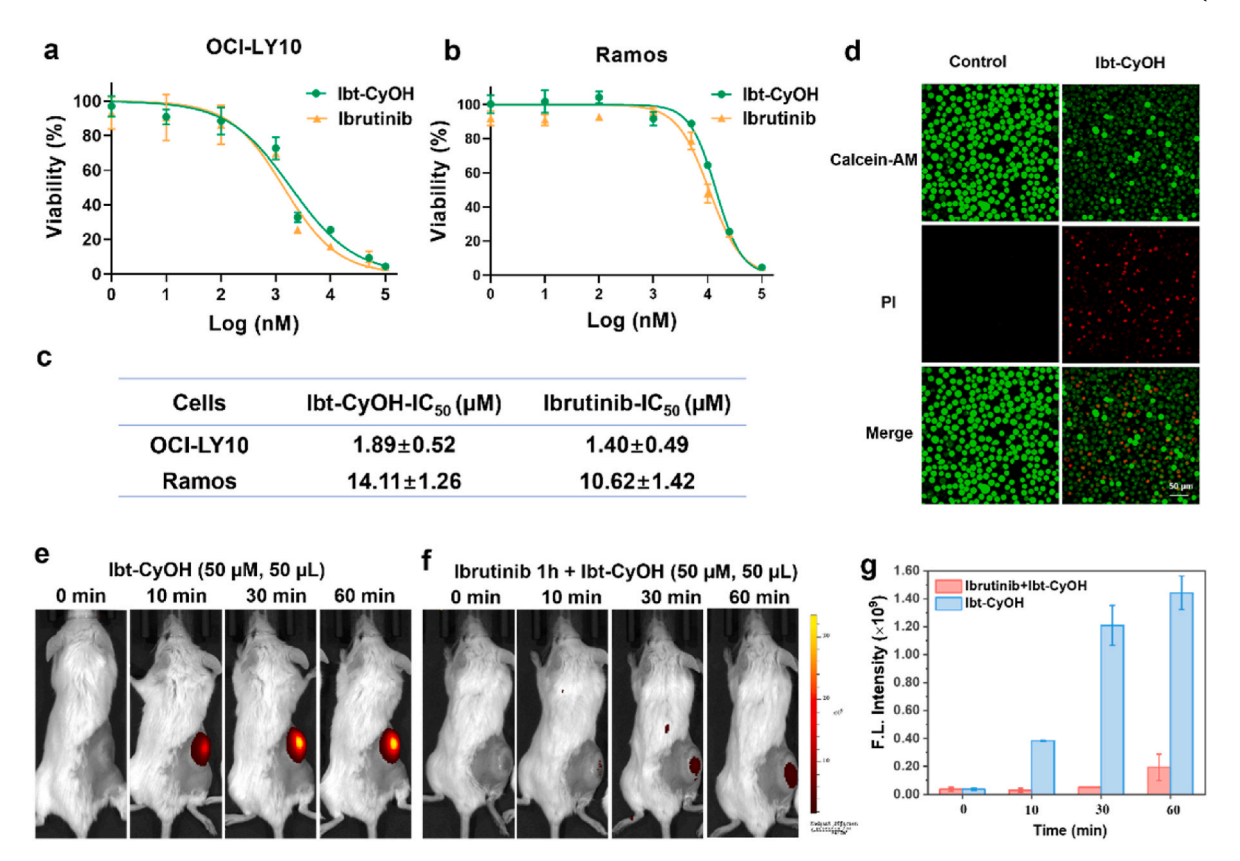


Fig. 4. Cell viability of Ibt-CyOH in (a) OCI-LY10 cells and (b) in Ramos cells. (c) 50 %-inhibitory effect on cell proliferation (IC₅₀, μ M), data are shown as mean \pm SD (n = 3). (d) Imaging of live/death OCI-LY10 cells incubated with Ibt-CyOH (10 μ M) using Calcien-AM/PI kit. (e) In vivo NIRF imaging of OCI-LY10 tumor-bearing mice upon intratumoral injection of Ibt-CyOH (50 μ M in 50 μ L of saline). (f) Intratumoral pre-injection of ibrutinib (100 μ M in 50 μ L of saline) for 1h, then injection of Ibt-CyOH (50 μ M in 50 μ L of saline). (i) Time-dependent NIRF intensity of tumor images of mice noted in panel (e,f). Data are shown as mean \pm SD (n = 3).

4. Conclusion

In summary, we have developed a BTK-activated NIRF probe, **Ibt-CyOH**, based on a targeted covalent binding-induced nucleophilic addition–elimination reaction that simultaneously achieves covalent inhibition and NIRF imaging of the targeted kinase for theranostics of in vivo B cell malignancies. The α -MAA linker between the guiding group and NIR fluorophore has been shown to serve multiple functions, including as an EW, a quencher of NIR fluorophore, and a cleavable linker induced by the nucleophilic addition–elimination reaction. Benefiting from the effect of targeted covalent inhibition, **Ibt-CyOH** exhibits high antiproliferative potency against B-cell malignancy cells, similar to that of the FDA-approved ibrutinib. We believe that the established promising targeted covalent activation strategy will inspire the development of new NIFR probes through the redesign of numerous FDA-approved targeted covalent drugs for theranostics of different cancers in the future.

CRediT authorship contribution statement

Xinyue Zhao: Methodology, Writing – original draft, Investigation, Conceptualization. Yuxin Gu: Methodology, Investigation. Yingyan Xie: Methodology, Investigation. Naijie Wei: Methodology, Investigation. Ziyang Fang: Methodology, Investigation. Xiaowen Yan: Investigation, Supervision, Writing – review & editing, Project administration, Conceptualization, Funding acquisition. Qiuquan Wang: Supervision, Funding acquisition, Writing – review & editing.

Declaration of competing interest

The authors declare that they have no known competing financial

interests or personal relationships that could have appeared to influence the work reported in this paper.

Acknowledgments

This study was financially supported by the National Natural Science Foundation of China (22074127, 22193053), the National Key Research and Development Program of China (2022YFF0710200), the Science and Technology Projects of Innovation Laboratory for Sciences and Technologies of Energy Materials of Fujian Province (IKKEM) (HRTP-[2022]-13), and the Fundamental Research Funds for the Central Universities (20720200073).

Appendix A. Supplementary data

Supplementary data to this article can be found online at https://doi.org/10.1016/j.bios.2025.117867.

Data availability

Data will be made available on request.

References

Aoki, Y., Isselbacher, K.J., Pillai, S., 1994. Proc. Natl. Acad. Sci. U. S. A. 91 (22), 10606–10609.

Buggy, J.J., Elias, L., 2012. Int. Rev. Immunol. 31 (2), 119-132.

Cao, C., Li, J., Zhang, X., Zhang, X., Gong, X., Wang, S., 2024. Talanta 272, 125786.
 Cao, R., Dang, Y., Liu, X., Sun, Q., Zhang, W., Xu, Z., 2025. Biosens. Bioelectron. 273, 117179.

Ceballos-Ávila, D., Vázquez-Sandoval, I., Ferrusca-Martínez, F., Jiménez-Sánchez, A., 2024. Biosens. Bioelectron. 264, 116638.

Chen, M., Yan, C., Zheng, L., Zhang, X.-E., 2022. Chem. Sci. 13 (4), 1119-1129.

- Chen, S., Tang, Y., Li, Y., Huang, M., Ma, X., Wang, L., Wu, Y., Wang, Y., Fan, W., Hou, S., 2023. Biosens. Bioelectron. 236, 115401.
- Christidi, E., Brunham, L.R., 2021. Cell Death Dis. 12 (4), 339.
- Degorce, S.L., Anjum, R., Dillman, K.S., Drew, L., Groombridge, S.D., Halsall, C.T., Lenz, E.M., Lindsay, N.A., Mayo, M.F., Pink, J.H., Robb, G.R., Scott, J.S., Stokes, S., Xue, Y., 2018. Biorg. Med. Chem. 26 (4), 913–924.
- Deng, M., Wang, P., Zhai, Z., Liu, Y., Cheng, D., He, L., Li, S., 2025. Anal. Chem. 97 (5), 2998–3008.
- Han, H.-H., Wang, H.-M., Jangili, P., Li, M., Wu, L., Zang, Y., Sedgwick, A.C., Li, J., He, X.-P., James, T.D., Kim, J.S., 2023. Chem. Soc. Rev. 52 (3), 879–920.
- Hong, G., Antaris, A.L., Dai, H., 2017. Nat. Biomed. Eng. 1 (1), 10.
- Honigberg, L.A., Smith, A.M., Sirisawad, M., Verner, E., Loury, D., Chang, B., Li, S., Pan, Z., Thamm, D.H., Miller, R.A., Buggy, J.J., 2010. Proc. Natl. Acad. Sci. U. S. A. 107 (29), 13075–13080.
- Kamle, M., Pandhi, S., Mishra, S., Barua, S., Kurian, A., Mahato, D.K., Rasane, P.,
 Büsselberg, D., Kumar, P., Calina, D., Sharifi-Rad, J., 2024. Med. Oncol. 41 (11), 263.
 Khan, W.N., 2001. Immunol. Res. 23 (2), 147–156.
- Kim, E., Yang, K.S., Kohler, R.H., Dubach, J.M., Mikula, H., Weissleder, R., 2015. Bioconjug. Chem. 26 (8), 1513–1518.
- Kraft, M.T., Pyle, R., Dong, X., Hagan, J.B., Varga, E., van Hee, M., Boyce, T.G., Pozos, T. C., Yilmaz-Demirdag, Y., Bahna, S.L., Abraham, R.S., 2021. Clin. Immunol. Ser. 229, 108788.
- Kumar, R., Shin, W.S., Sunwoo, K., Kim, W.Y., Koo, S., Bhuniya, S., Kim, J.S., 2015.
 Chem. Soc. Rev. 44 (19), 6670–6683.
- Li, H., Kim, H., Xu, F., Han, J., Yao, Q., Wang, J., Pu, K., Peng, X., Yoon, J., 2022. Chem. Soc. Rev. 51 (5), 1795–1835.
- Li, J., Van Valkenburgh, J., Hong, X., Conti, P.S., Zhang, X., Chen, K., 2019. Theranostics 9 (25), 7849–7871.
- 9 (25), 7849–7871. Li, W., Sun, L., Zheng, X., Li, F., Zhang, W., Li, T., Guo, Y., Tang, D., 2023. Anal. Chem.
- 95 (25), 9654–9662. Liu, C., Wang, X., Zhu, H., Wang, K., Yu, M., Zhang, Y., Su, M., Rong, X., Sheng, W., Zhu, B., 2023. Anal. Chem. 95 (31), 11732–11740.
- Liu, H.-W., Hu, X.-X., Li, K., Liu, Y., Rong, Q., Zhu, L., Yuan, L., Qu, F.-L., Zhang, X.-B., Tan, W., 2017. Chem. Sci. 8 (11), 7689–7695.
- Liu, N., Hoogendoorn, S., van de Kar, B., Kaptein, A., Barf, T., Driessen, C., Filippov, D.V., van der Marel, G.A., van der Stelt, M., Overkleeft, H.S., 2015. Org. Biomol. Chem. 13 (18), 5147–5157.
- Lonsdale, R., Ward, R.A., 2018. Chem. Soc. Rev. 47 (11), 3816-3830.
- Owens, E.A., Henary, M., El Fakhri, G., Choi, H.S., 2016. Acc. Chem. Res. 49 (9), 1731–1740.
- Pal Singh, S., Dammeijer, F., Hendriks, R.W., 2018. Mol. Cancer 17 (1).
- Pan, Z., Scheerens, H., Li, S.-J., Schultz, B.E., Sprengeler, P.A., Burrill, L.C., Mendonca, R. V., Sweeney, M.D., Scott, K.C.K., Grothaus, P.G., Jeffery, D.A., Spoerke, J.M., Honigberg, L.A., Young, P.R., Dalrymple, S.A., Palmer, J.T., 2007. ChemMedChem 2 (1), 58–61.

- Reddi, R.N., Resnick, E., Rogel, A., Rao, B.V., Gabizon, R., Goldenberg, K., Gurwicz, N., Zaidman, D., Plotnikov, A., Barr, H., Shulman, Z., London, N., 2021. J. Am. Chem. Soc. 143 (13), 4979–4992.
- Satterthwaite, A.B., Cheroutre, H., Khan, W.N., Sideras, P., Witte, O.N., 1997. Proc. Natl. Acad. Sci. U. S. A. 94 (24), 13152–13157.
- Sharma, A., Verwilst, P., Li, M., Ma, D., Singh, N., Yoo, J., Kim, Y., Yang, Y., Zhu, J.-H., Huang, H., Hu, X.-L., He, X.-P., Zeng, L., James, T.D., Peng, X., Sessler, J.L., Kim, J.S., 2024. Chem. Rev. 124 (5), 2699–2804.
- Song, J., Zhai, T., Hahm, H.S., Li, Y., Mao, H., Wang, X., Jo, J., Chang, J.W., 2024. Angew. Chem. Int. Ed. 63 (40), e202410645.
- Tseng, W.-B., Chou, Y.-S., Lu, C.-Z., Madhu, M., Lu, C.Y., Tseng, W.-L., 2021. Biosens. Bioelectron. 193, 113522.
- Wang, L., Sun, T., Zhen, T., Li, W., Yang, H., Wang, S., Feng, F., Chen, Y., Sun, H., 2024.
 J. Med. Chem. 67 (8), 6793–6809.
- Wang Michael, L., Rule, S., Martin, P., Goy, A., Auer, R., Kahl Brad, S., Jurczak, W., Advani Ranjana, H., Romaguera Jorge, E., Williams Michael, E., Barrientos Jacqueline, C., Chmielowska, E., Radford, J., Stilgenbauer, S., Dreyling, M., Jedrzejczak Wieslaw, W., Johnson, P., Spurgeon Stephen, E., Li, L., Zhang, L., Newberry, K., Ou, Z., Cheng, N., Fang, B., McGreivy, J., Clow, F., Buggy Joseph, J., Chang Betty, Y., Beaupre Darrin, M., Kunkel Lori, A., Blum Kristie, A., 2023. N. Engl. J. Med. 369 (6), 507–516.
- Wang, T., Li, S., Zou, Z., Hai, L., Yang, X., Jia, X., Zhang, A., He, D., He, X., Wang, K., 2018. J. Mater. Chem. B 6 (23), 3914–3921.
- Wei, W., Huang, C., Zhang, J., Chen, Q., Liu, Z., Ren, X., Gan, S., Wu, P., Wang, D., Tang, B.Z., Sun, H., 2024. Anal. Chem. 96 (6), 2406–2414.
- Woyach, J.A., Johnson, A.J., Byrd, J.C., 2012. Blood 120 (6), 1175-1184.
- Wu, X., Li, L., Shi, W., Gong, Q., Ma, H., 2016. Angew. Chem. Int. Ed. 55 (47), 14728–14732.
- Wu, X., Sun, X., Guo, Z., Tang, J., Shen, Y., James, T.D., Tian, H., Zhu, W., 2014. J. Am. Chem. Soc. 136 (9), 3579–3588.
- Xue, H., Wang, X., Jiang, Q., Ma, J., Wong, M.S., 2025. Biosens. Bioelectron. 275, 117201.
- Ye, M., Wang, X., Tang, J., Guo, Z., Shen, Y., Tian, H., Zhu, W.-H., 2016. Chem. Sci. 7 (8), 4958–4965.
- Yin, J., Huang, L., Wu, L., Li, J., James, T.D., Lin, W., 2021. Chem. Soc. Rev. 50 (21), 12098–12150.
- Zhang, J., Ning, L., Huang, J., Zhang, C., Pu, K., 2020. Chem. Sci. 11 (3), 618-630.
- Zhang, Q., Liu, H., Pan, Z., 2014. Chem. Commun. 50 (97), 15319–15322.
- Zhao, X.-b., Gao, K., Shi, Y.-p., 2021. Anal. Chem. 93 (45), 15080-15087.
- Zhou, R., Liu, G., Fu, S., Zheng, H., Li, D., Dai, J., Wei, J., Li, B., Wang, C., Lu, G., 2024. Biosens. Bioelectron. 264, 116624.
- Zhu, L., Chen, L., 2019. Cell. Mol. Biol. Lett. 24, 40.
- Zhuang, J., Zhao, B., Meng, X., Schiffman, J.D., Perry, S.L., Vachet, R.W., Thayumanavan, S., 2020. Chem. Sci. 11 (8), 2103–2111